

---

# Design of a creep resistant nickel base superalloy for power plant applications

## Part 1 – Mechanical properties modelling

F. Tancret, H. K. D. H. Bhadeshia and D. J. C. MacKay

Models have been developed and used as tools to design a new ‘made to measure’ nickel base superalloy for power plant applications. In Part 1, Gaussian processes are used to model the tensile and creep rupture properties of superalloys as a function of their composition and processing parameters, making use of large databases on existing alloys. The models are able to estimate the actual influence of alloying elements on the mechanical properties over a wide range of temperature and stress. They have been used, in conjunction with general metallurgical concepts and industrial requirements, as a basis for the design of a new Ni–Cr–W–Al–Ti–Fe–Si–C–B superalloy with desirable properties. It is estimated that the proposed forgeable and weldable alloy should have a creep rupture life at 750°C of 100 000 h under a stress of 100 MPa, with a huge reduction in price compared to existing commercial alloys with similar properties. In a following paper, Part 2, an attempt is made to design against the formation of undesirable phases and chemical segregation, using phase diagram calculations. Preliminary experimental results are presented in Part 3.

MST/5389

*Dr Tancret is in the Laboratoire Génie des Matériaux, Polytech' Nantes, La Chantrerie–Rue Christian Pauc, BP 50609, 44306 Nantes Cedex 3, France (franck.tancret@polytechuniv-nantes.fr). Professor Bhadeshia is in the Department of Materials Science and Metallurgy, University of Cambridge, Pembroke Street, Cambridge CB2 3QZ, UK. Dr MacKay is in the Department of Physics, Cavendish Laboratory, University of Cambridge, Madingley Road, Cambridge CB3 0HE, UK. Manuscript received 29 January 2002; accepted 18 September 2002.*

© 2003 IoM Communications Ltd. Published by Maney for the Institute of Materials, Minerals and Mining.

---

### Introduction

Future fossil fuel power plants are being conceived to operate with steam temperatures as high as 750°C. This is expected to increase the thermodynamic cycle efficiency from 42% with the present typical temperature of 600°C, to 60%, providing huge fuel savings as well as a significant reduction of polluting emissions. Although ferritic steels may remain usable at temperatures approaching 650°C, other materials having superior creep properties will be needed for higher temperatures. Austenitic stainless steels may be used in thin walled components but they suffer from a high thermal expansion coefficient and a low thermal conductivity. For this reason, nickel base superalloys are currently the prime candidates for temperatures in excess of 650°C, but the price of commercially available alloys is considered too high for large scale power plant applications. These current alloys contain expensive alloying elements such as Mo, Co, Ta, Nb, or even Hf, Re...

The aim of the present work is to propose a new nickel base alloy, with composition and heat treatment, compatible with good high temperature mechanical properties and reduced price (based on the cost of alloying elements) compared to commercially available superalloys. The typical requirement is a creep rupture life of 100 000 h at 750°C under a stress of 100 MPa. It should also be forgeable, weldable, oxidation resistant, and its microstructure should be stable over long exposures at service temperature.

However, because the influence of the composition and processing parameters on the material properties is extremely complex and multivariate, designing an alloy ‘to measure’ is not feasible using experience alone. Modern alloys contain many chemical elements added to achieve particular properties. The influence of individual alloying elements on mechanical properties can be measured and understood in isolated cases; simple interactions between two or three elements can be formulated, but describing all the interactions as a whole is generally impossible. For this

reason, various modelling techniques have been used to predict the mechanical properties of alloys, microstructural parameters, and high temperature phase stability. They include Gaussian processes (non-linear multidimensional statistical regression analyses) and phase diagram simulations. These tools have been used to propose a new alloy that should possess the required mechanical properties and a stable microstructure that avoids the formation of undesirable phases. Part 1 of this series of papers deals with the Gaussian processes modelling of mechanical properties. Part 2 will deal with phase formation, chemical segregation simulation, and processing. Preliminary results on a semi-industrial scale sample are presented in Part 3.

---

### Gaussian processes modelling

Recent papers<sup>1–4</sup> have demonstrated the possibility of using Gaussian processes to model the properties of complex materials as a function of their composition and/or processing parameters. They perform a non-linear multidimensional regression of an output (a mechanical, physical, or microstructural property...) as a function of many inputs (composition, thermomechanical treatments, temperature, etc.). Ideally, the database on which the model is based must contain a large number of measurements, covering a wide range of alloy compositions and test conditions.

---

### THEORETICAL BACKGROUND

First, the statistical structure of Gaussian processes is presented.<sup>5,6</sup> Consider the data  $D$  as constituted of  $N$   $L$ -dimensional input vectors  $\{\vec{x}_1, \vec{x}_2, \dots, \vec{x}_N\} = [X_N]$ , each vector referring to one alloy tested in particular conditions, and their  $N$  corresponding outputs or targets  $\{t_1, t_2, \dots, t_N\} = \vec{t}_N$ , each target being a measurement. The joint probability distribution, in an  $N$ -dimensional space, of the target vector  $\vec{t}_N$  given the input matrix  $[X_N]$ , is denoted

$P(\vec{t}_N|[X_N])$ . To predict the output value,  $t_{N+1}$ , corresponding to a new input vector,  $\vec{x}_{N+1}$  (i.e. a new alloy and/or new test conditions), it is required to calculate the one dimensional probability distribution over the predicted point  $P(t_{N+1}|\vec{x}_{N+1}, D)$ , given a knowledge of the corresponding input vector,  $\vec{x}_{N+1}$ , and the data  $D = \{\vec{t}_N, [X_N]\}$ . The latter is related to the joint probability distribution of both the  $N$  data points and of the new point,  $P(t_{N+1}, \vec{t}_N|\vec{x}_{N+1}, [X_N])$  by the following relationship<sup>5</sup>

$$P(t_{N+1}|\vec{x}_{N+1}, D) = \frac{P(t_{N+1}, \vec{t}_N|\vec{x}_{N+1}, [X_N])}{P(\vec{t}_N|[X_N])} \quad (1)$$

This distribution is defined to be a Gaussian process. The model assumes that the joint probability distribution of any  $N$  output values is a multivariate Gaussian,

$$P(\vec{t}_N|[X_N], \Theta) \propto \exp\left(-\frac{1}{2}(\vec{t}_N - \vec{v})^T [C_N]^{-1}(\vec{t}_N - \vec{v})\right) \quad (2)$$

where  $\vec{v}$  is the mean,  $[C_N]$  a covariance matrix which is a function of  $[X_N]$ , and  $\Theta$  a set of parameters that will be discussed later. A similar equation with  $N+1$  variables holds for  $\vec{t}_{N+1} = (t_{N+1}, \vec{t}_N)$ , and equation (1) reduces to a univariate Gaussian of the form<sup>5</sup>

$$P(t_{N+1}|\vec{x}_{N+1}, D) = \frac{1}{\sqrt{2\pi}\sigma_{\hat{t}}} \exp\left[-\frac{(t_{N+1} - \hat{t})^2}{2\sigma_{\hat{t}}^2}\right] \quad (3)$$

where  $\hat{t}$  is the posterior mean, i.e. the prediction, and  $\sigma_{\hat{t}}$  its standard deviation given by

$$\hat{t} = [k]^T [C_N]^{-1} \vec{t}_N \quad (4)$$

and

$$\sigma_{\hat{t}}^2 = k - [k]^T [C_N]^{-1} [k] \quad (5)$$

where

$$[k] = [C(\vec{x}_1, \vec{x}_{N+1}), C(\vec{x}_2, \vec{x}_{N+1}), \dots, C(\vec{x}_N, \vec{x}_{N+1})] \quad (6)$$

and

$$k = C(\vec{x}_{N+1}, \vec{x}_{N+1}) \quad (7)$$

Equation (3) gives the probability distribution of the new output  $t_{N+1}$  given the new set of inputs  $\vec{x}_{N+1}$  and the data  $D$ . Both the prediction  $\hat{t}$  and its standard deviation  $\sigma_{\hat{t}}$  depend on the covariance matrix  $[C_N]$  whose elements  $C_{ij}$  are given by the covariance function  $C$ . The form of this function is essential since it embodies the assumptions about the nature of the underlying input-output function it is required to model. Basically, it defines how strongly any

input will influence the value of the output, and the lengthscales of trends in the function underlying the data. The covariance function used is

$$C(\vec{x}_i, \vec{x}_j|\Theta) = \theta_1 \exp\left[-\frac{1}{2} \sum_{\ell=1}^L \frac{(x_i^\ell - x_j^\ell)^2}{r_\ell^2}\right] + \theta_2 + \sigma_n^2 \delta_{ij} \quad (8)$$

where  $\Theta = \{r_\ell (\ell = 1 \text{ to } L), \theta_1, \theta_2, \sigma_n\}$ .

This function gives the covariance between any two outputs,  $t_i$  and  $t_j$ , with corresponding input vectors  $\vec{x}_i$  and  $\vec{x}_j$ . The closer the inputs, the smaller the exponent of the first term in equation (8), the larger the first term, and the stronger the outputs will be correlated, making it probable that they have similar values. This first term also includes the length scale  $r_\ell$  over which the function varies in the  $\ell$ th input dimension, which is an indication of the smoothness of the interpolant in this dimension. This covariance function expects there to be no long range correlations in the data on lengthscales much bigger than  $r_\ell$ .

The second term  $\theta_2$  is an offset, allowing the functions to have a non-zero mean value. The last term,  $\sigma_n^2 \delta_{ij}$ , is the noise model, with  $\delta_{ij}$  being equal to 1 if  $i=j$  and to 0 otherwise. We have thus an input-independent noise model of variance  $\sigma_n^2$  for the output, and we are assuming the inputs to be noise free.

The set of parameters  $\Theta = \{r_\ell (\ell = 1 \text{ to } L), \theta_1, \theta_2, \sigma_n\}$  are called the *hyperparameters* because they define the probability distribution over functions rather than the interpolating function itself. The hyperparameters  $\Theta$ , the dataset  $[X_N]$ ,  $\vec{t}_N$ , and the new input vector  $\vec{x}_{N+1}$ , define completely the value of the prediction  $\hat{t}$  and of its standard deviation  $\sigma_{\hat{t}}$ . The optimum values of the hyperparameters are inferred during the training of the model by maximising the probability of the hyperparameters given the data  $P(\Theta|D)$ , which is done numerically within a Bayesian framework.<sup>5</sup>

## DATABASES

The data have been collected from industrial sources and from the scientific literature. They concern mechanical properties: yield stress  $Y$ , ultimate tensile stress UTS, tensile ductility, creep rupture stress CRS; and the  $\gamma$  and  $\gamma'$  lattice parameters  $a_\gamma$  and  $a_{\gamma'}$ . The databases contain information on the alloy compositions, on the heat and/or mechanical treatments, and on test conditions temperature and lifetime in the case of creep rupture.

Tables 1 and 2 present the inputs used for the different modelling problems, as well as their range in the databases.

**Table 1 Nature and range of chemical composition inputs in database**

| Input | Unit  | Y         | UTS       | Ductility | log CRS   | $a_\gamma$ | $a_{\gamma'}$ |
|-------|-------|-----------|-----------|-----------|-----------|------------|---------------|
| Ni    |       | ...       | ...       | ...       | ...       | 31.1-100   | 32-90.2       |
| Cr    |       | 5.7-30    | 5.7-30    | 5.7-30    | 5.7-30    | 0-34.8     | 0-34.8        |
| Co    |       | 0-20      | 0-20      | 0-20      | 0-20.1    | 0-68.9     | 0-25          |
| Mo    |       | 0-14.5    | 0-14.5    | 0-14.5    | 0-14.5    | 0-26.51    | 0-4.82        |
| W     |       | 0-12      | 0-12      | 0-12      | 0-12      | 0-15.5     | 0-4.87        |
| Ta    |       | 0-9       | 0-9       | 0-9       | 0-9       | 0-8.019    | 0-10.14       |
| Nb    |       | 0-6.5     | 0-6.5     | 0-6.5     | 0-6       | 0-7.9      | 0-8.03        |
| Al    |       | 0-6.5     | 0-6.5     | 0-6.5     | 0-6.5     | 0-17       | 0-26          |
| Ti    |       | 0-5       | 0-5       | 0-5       | 0-5       | 0-9.5      | 0-20          |
| Fe    |       | 0-57.79   | 0-57.79   | 0-57.79   | 0-57.79   | 0-35       | 0-64          |
| Mn    | wt.-% | 0-1.24    | 0-1.24    | 0-1.24    | 0-1.25    | ...        | ...           |
| Si    |       | 0-2.35    | 0-2.35    | 0-2.35    | 0-2.35    | ...        | ...           |
| C     |       | 0.02-0.35 | 0.02-0.35 | 0.02-0.35 | 0.02-0.35 | ...        | ...           |
| B     |       | 0-0.16    | 0-0.16    | 0-0.16    | 0-0.16    | ...        | ...           |
| Zr    |       | 0-0.6     | 0-1       | 0-1       | 0-1       | ...        | ...           |
| Cu    |       | 0-0.21    | 0-0.21    | 0-0.21    | 0-0.56    | 0-32.41    | ...           |
| N     |       | 0-0.017   | 0-0.017   | 0-0.017   | 0-0.04    | ...        | ...           |
| S     |       | 0-0.009   | 0-0.009   | 0-0.009   | 0-0.05    | ...        | ...           |
| P     |       | 0-0.006   | 0-0.006   | 0-0.006   | 0-0.011   | ...        | ...           |
| V     |       | 0-1       | 0-1       | 0-1       | 0-1       | 0-41.92    | 0-10          |
| Hf    |       | ...       | ...       | ...       | ...       | 0-1.12     | 0-4.038       |
| Re    |       | ...       | ...       | ...       | ...       | 0-2.67     | 0-0.25        |
| Ga    |       | ...       | ...       | ...       | ...       | 0-15.72    | 0-29.8        |
| Au    |       | ...       | ...       | ...       | ...       | 0-6.7      | ...           |

All the inputs and outputs have been normalised linearly between  $-0.5$  and  $+0.5$ , corresponding respectively to the lowest and the highest value of each input or output in the database. This allows an easier visualisation of the importance of each variable in explaining changes in the output parameter, and better computing efficiency.

## MODELLING AND TEST

Once the models have been trained, it is necessary, before using them, to make predictions in order to test their validity, i.e. to check that they are able to make correct predictions in cases where the output is known, for example, for the points of the database or where the actual trends are known theoretically or experimentally. It is not the aim here to present an exhaustive list of tested trends, but to show a few examples to illustrate the testing procedure.

### Training and test

Figure 1 shows comparisons between the measured properties and those predicted by the models for the points contained in the databases, i.e. used to create the models. A small dispersion of the points around the ' $x=y$ ' line means a small error, i.e. a good prediction. The error bars given by Gaussian processes correspond to the  $1\sigma$  dispersion of the calculated probability distribution of the output calculated by equation (5), and include both the predictive uncertainty and the noise level in the database  $\sigma_n$  of equation (8). In all cases a good alignment of points along the ' $x=y$ ' line is obtained, with reasonable error bars. It is worth noting that in the case of creep rupture stress, error bars increase systematically with increasing CRS values, which is a consequence of log CRS being modelled and not CRS itself. The overall aspect of these graphs is satisfactory, and represents both a necessary step and a good first result.

### Temperature and stress

Ni base superalloys are often comprised of a dual phase microstructure in which  $Ni_3(Al,Ti)$  intermetallic precipitates, designated  $\gamma'$ , are embedded in a disordered face centred cubic solid solution  $\gamma$ . Both phases can contain solute elements, such as Mo, Co, Cr, Fe (mainly in  $\gamma$ ), Ta, Nb ( $\gamma'$ ), and W (in both phases). The  $\gamma$  phase softens as temperature increases, but the  $\gamma'$  phase first hardens up to about  $900^\circ\text{C}$ , and then softens. Depending of the volume fraction of  $\gamma'$  precipitates, this competition between softening and hardening phase often results in a particular peak effect in the plot of the yield stress versus temperature,<sup>7</sup> as presented in Fig. 2 for Nimonic 115 (Ni-14.3Cr-13.2Co-3.3Mo-4.9Al-3.7Ti-0.15C-0.16B-0.04Zr (wt-%)). The Gaussian processes predicted trend is also presented in this

graph, and is in good agreement with the actual measurements. It can be noted that the error bars become large in the temperature range  $21-500^\circ\text{C}$ , which is a region of the database where no measurements are available. Error bars act as a warning signal indicating that the model is not confident in this domain.

Another consequence of this anomalous strengthening is the evolution of ductility with temperature, as shown on Fig. 3 for Nimonic 90 (Ni-19.5Cr-16.5Co-1.45Al-2.45Ti-0.3Mn-0.3Si-0.07C-0.003B-0.06Zr). Whereas for 'normal' metals ductility monotonically increases with temperature, due to continuous softening, the ductility of aged Ni base superalloys passes through a minimum when the discrepancy between the plastic flow properties of the two phases is maximum, which favours failure initiation, and then increases as the  $\gamma'$  inclusions soften and finally progressively dissolve above the  $\gamma'$  solvus, typically above  $1000^\circ\text{C}$ . This behaviour is also well predicted by the Gaussian processes model (Fig. 3).

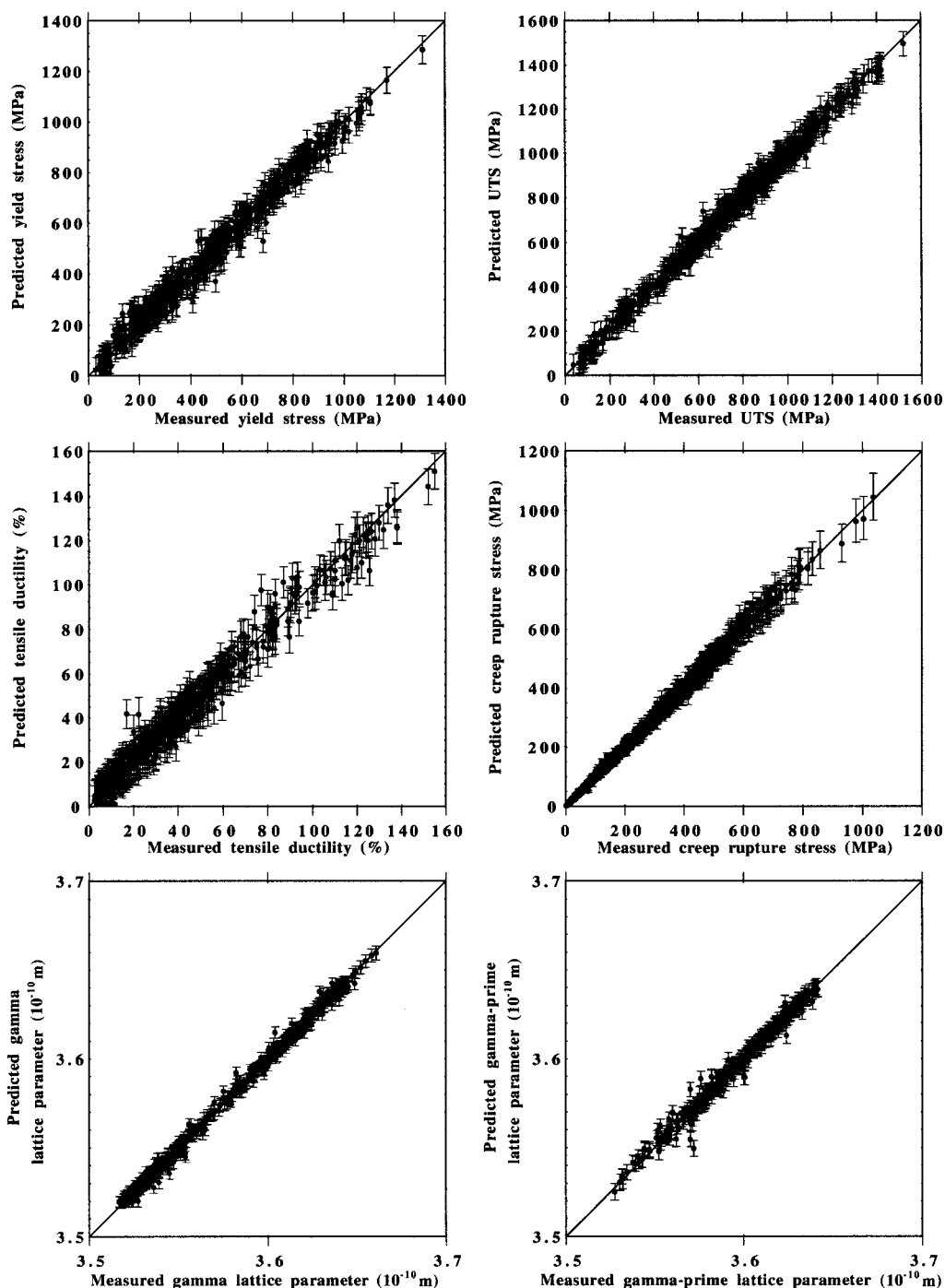
Creep rupture is a very complex phenomenon since it embodies the whole deformation history of the material during the three commonly accepted stages of creep: primary creep where dislocation structures and substructures build up, and where damage initiation is sometimes observed; secondary creep where the structure and deformation rates are roughly constant, and where damage nucleation continues; and tertiary creep where damage grows, clusters, and ends in the propagation of a macroscopic crack. Also, due to high temperature exposure and deformation, the microstructure itself is likely to evolve (grain growth, carbide precipitation and/or dissolution, rafting, etc.). Consequently, creep rupture is one of the typical metallurgical problems where physical models do not yet describe the process as a whole. On the other hand, empirical models based on data analysis, e.g. Gaussian processes or artificial neural networks, are, at present, the only efficient way to perform reliable predictions, because, in dealing directly with raw data, they take all underlying parameters into account. In this respect, the present Gaussian processes model has proved to be able to predict correctly the creep rupture behaviour of materials not included in the database. For example, Fig. 4 shows the accurately predicted relation between the creep rupture stress and lifetime at  $870^\circ\text{C}$  of an IN939 superalloy (Ni-22.4Cr-19Co-2W-1.4Ta-1Nb-1.9Al-3.7Ti-0.15C-0.01B-0.1Zr).<sup>8</sup>

### $\gamma'$ formers: Al and Ti

Aluminium and titanium play a major role in the mechanical properties of Ni base superalloys because they form the coherent intermetallic precipitates  $Ni_3(Al,Ti)$ , or  $\gamma'$ . The

**Table 2** Nature and range of the process inputs and of the outputs in the database. The  $t_i$  and  $T_i$  inputs correspond to the duration and temperature of heat treatments:  $i=1$  and 2 correspond to the first and second 'high temperature' heat treatments, 3 and 4 to the first and second 'low temperature' heat treatments (aging)

| Input          | Unit                   | Y       | UTS     | Ductility | log CRS        | $a_i$         | $a_i$         |
|----------------|------------------------|---------|---------|-----------|----------------|---------------|---------------|
| Forged         | Binary:                | 0-1     | 0-1     | 0-1       | 0-1            | ...           | ...           |
| Cold deformed  | 0=no, 1=yes            | ...     | ...     | ...       | 0-1            | ...           | ...           |
| $t_1$          | h and $^\circ\text{C}$ | 0-8     | 0-8     | 0-8       | 0-8            | ...           | ...           |
| $T_1$          |                        | 0-1235  | 0-1235  | 0-1235    | 0-1235         | ...           | ...           |
| $t_2$          |                        | 0-16    | 0-16    | 0-16      | 0-16           | ...           | ...           |
| $T_2$          |                        | 0-1100  | 0-1100  | 0-1100    | 0-1100         | ...           | ...           |
| $t_3$          |                        | 0-50    | 0-50    | 0-50      | 0-50           | ...           | ...           |
| $T_3$          |                        | 0-870   | 0-870   | 0-870     | 0-925          | ...           | ...           |
| $t_4$          |                        | 0-24    | 0-24    | 0-24      | 0-24           | ...           | ...           |
| $T_4$          |                        | 0-760   | 0-760   | 0-760     | 0-760          | ...           | ...           |
| T              | $^\circ\text{C}$       | 20-1093 | 20-1093 | 20-1093   | 500-1149       | 15-1100       | 20-1100       |
| log $t_i$      | $t_i$ in h             | ...     | ...     | ...       | 0.6721-4.0938  | ...           | ...           |
| Output (unit)  |                        | 28-1310 | 35-1520 | 2.5-155   | 0.30103-3.0149 | 3.5166-3.6606 | 3.5273-3.6415 |
|                |                        | (MPa)   | (MPa)   | (%)       | (CRS in MPa)   | ( $\bar{A}$ ) | ( $\bar{A}$ ) |
| Number of data |                        | 642     | 656     | 638       | 1816           | 455           | 311           |



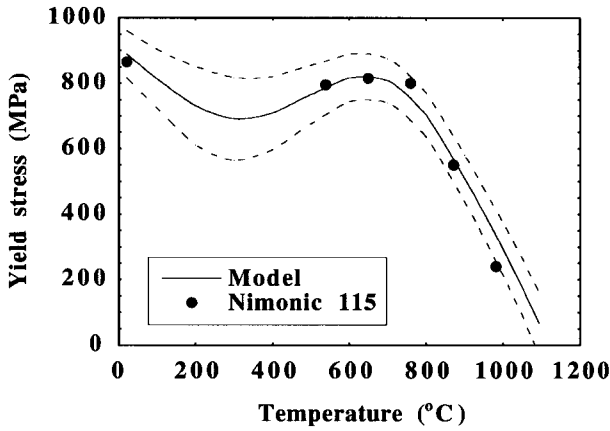
1 Graphs of predicted versus measured values for points in the databases (yield stress, ultimate tensile stress, tensile ductility, creep rupture stress,  $\gamma$  and  $\gamma'$  lattice parameters)

predicted influences of Ti and Al additions on the yield strength at 20°C, and on the  $10^5$  h creep rupture stress at 750°C, of a Ni–20Cr–10Co–0.03C alloy, are presented in Fig. 5. In agreement with theoretical considerations, these elements increase both properties, by creating obstacles to dislocation motion. However, the respective influence of Al and Ti on the yield stress and on the creep rupture stress seems inverted. Indeed, since titanium atoms are bigger than aluminium (+4%), they induce an increase in the  $\gamma'$  lattice parameter and the  $\gamma/\gamma'$  lattice mismatch, and thus of the strain fields. It also increases the antiphase boundary energy of the  $\gamma'$  phase, which renders more difficult the cutting of inclusions by dislocations at low temperatures.<sup>9,10</sup> Titanium is thus expected to give more effective strengthening effects on the yield stress than aluminium, and this has been

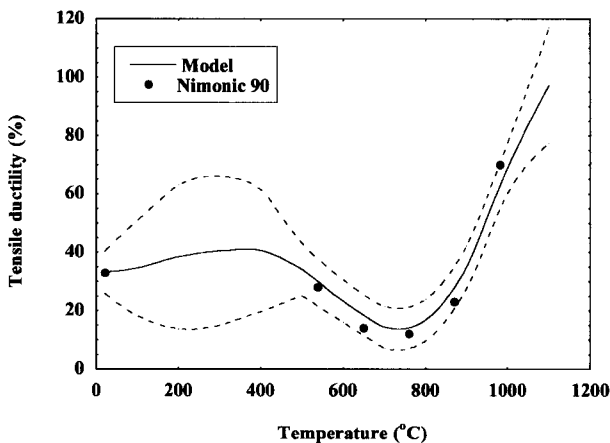
recognised by the Gaussian processes. On the other hand, it has been shown that increasing the  $\gamma/\gamma'$  lattice misfit deteriorates the creep resistance.<sup>11</sup> Thus, adding titanium, even if it increases the creep resistance by promoting  $\gamma'$  precipitation, is less effective than aluminium because of a higher lattice misfit, which is also predicted by the model.

### Co, Mo, and W

The predicted influence of Co, Mo, and W on the  $10^5$  h creep rupture stress at 750°C of a Ni–20Cr–10Co–1Al–1Ti–0.03C alloy is presented in Fig. 6. All these elements increase the creep resistance of Ni base superalloys, in agreement with known results.<sup>12,13</sup> However, because they partition differently to the  $\gamma$  and  $\gamma'$  phases,<sup>14</sup> their

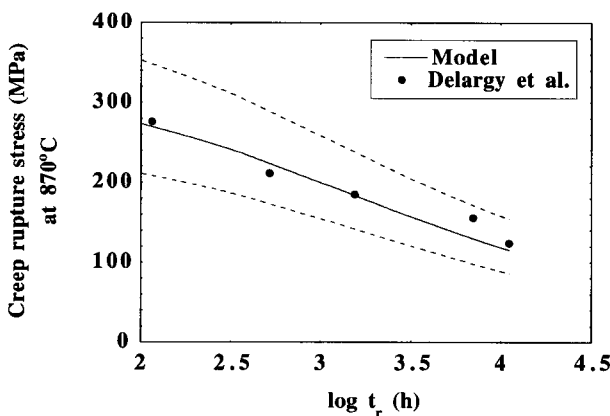


2 Predicted and actual evolution of yield stress of Nimonic 115 superalloy with temperature: experimental points were included in database during model training

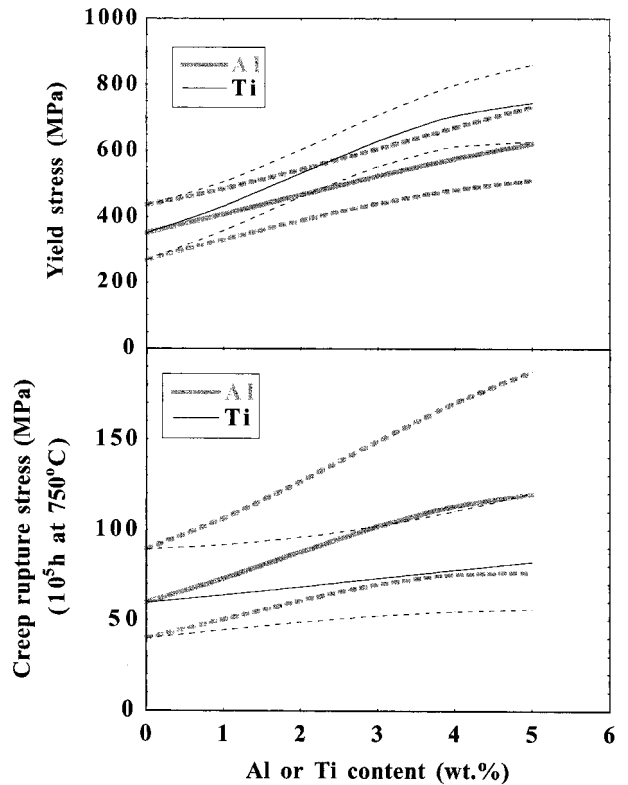


3 Predicted and actual evolution of tensile ductility of Nimonic 90 superalloy with temperature: experimental points were included in database during model training

strengthening mechanisms are different. Cobalt and molybdenum partition mainly to the  $\gamma$  phase, hence giving a solid solution strengthening of the matrix. Tungsten partitions about equally to  $\gamma$  and  $\gamma'$ , and yields both a solid solution strengthening of the matrix<sup>15</sup> and an increase of the antiphase boundary energy of the inclusions.<sup>16</sup> However, the latter effect, if it contributes to the increase in yield



4 Predicted and actual relation between creep rupture stress of IN939 superalloy and its lifetime at 870°C: experimental points from Ref. 8 were not included in the database during model training



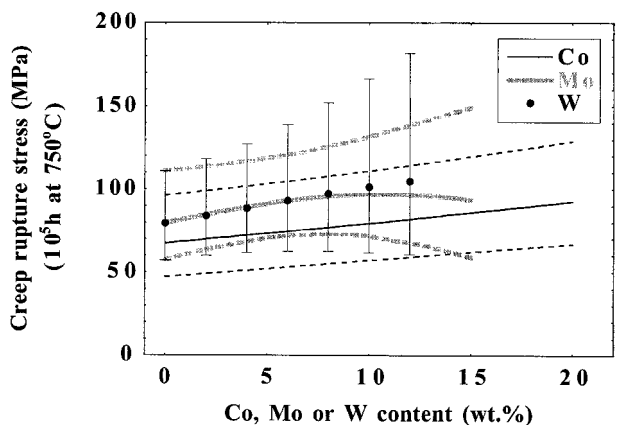
5 Predicted influence of Al and Ti additions on room temperature yield stress and  $10^5$  h creep rupture stress at 750°C of Ni-20Cr-10Co-0.03C (wt-%) alloy heat treated for 1 h at 1175°C and 8 h at 800°C

stress, has little influence on long term creep resistance, where the deformation mechanism is dislocation climb around precipitates.

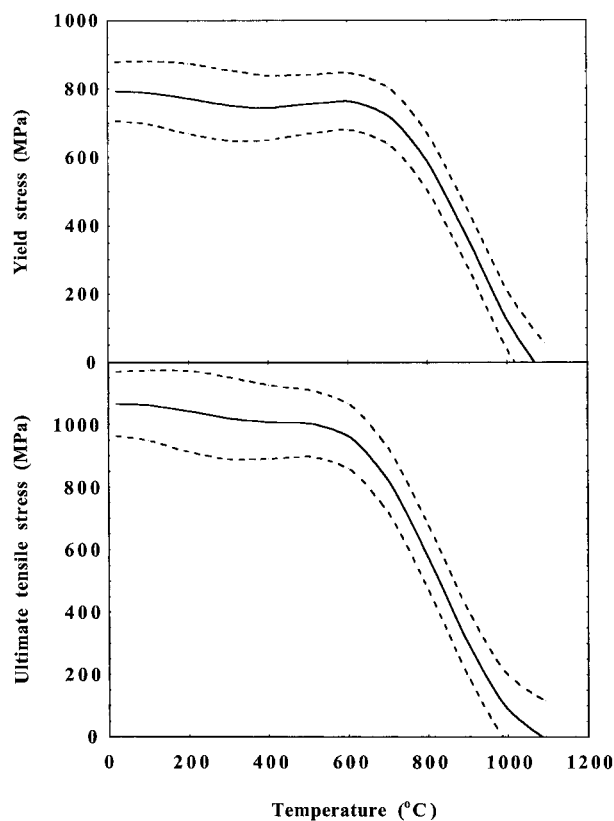
## Alloy design

### GENERAL CONCEPTS

The engineering requirements dictate a creep rupture life of 100 000 h at 750°C under a stress of 100 MPa, but there are other important design features that must be satisfied simultaneously. The UTS to Y ratio should be as high as possible, and in any case in excess of 1.3 at room temperature. The alloy must be easily forgeable and workable,



6 Predicted influence of Co, Mo and W content on  $10^5$  h creep rupture stress at 750°C of Ni-20Cr-10Co-1Al-1Ti-0.03C (wt-%) alloy heat treated for 1 h at 1175°C and 8 h at 800°C



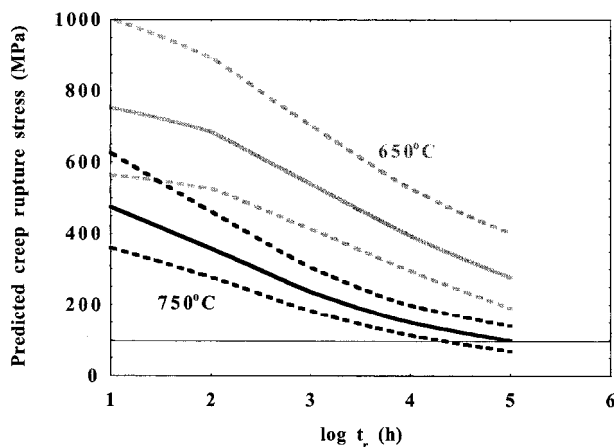
7 Predicted yield stress and ultimate tensile stress of proposed alloy as function of temperature

i.e. it must be free of  $\gamma'$  for all temperatures within  $\sim 200$  K of melting. Furthermore, the quantity of  $\gamma'$  must be less than  $\sim 25\%$  by volume after heat treatment in order to ensure weldability<sup>17</sup> and ductility. Naturally, any such alloy must be able to cope with corrosive environments.

An essential purpose of this work was price reduction with respect to existing alloys, which means that expensive elements such as Co, Mo, Ta, Nb, Hf and Re must be avoided, or their use optimised. Consequently, the proposed alloy contained the following elements.

- (i) high chromium content, typically 20 wt-%, to achieve a good high temperature corrosion resistance
- (ii) aluminium and titanium to form  $\gamma'$  precipitates, hence providing a precipitation strengthening effect. Their relative amounts must be adjusted to achieve a low  $\gamma/\gamma'$  lattice misfit. Ti increases the misfit and Al decreases it<sup>18</sup>
- (iii) tungsten, to induce solid solution strengthening of both the  $\gamma$  matrix and  $\gamma'$  precipitates<sup>13</sup>
- (iv) carbon, to precipitate grain boundary carbides, which limit grain boundary sliding. Its content must, however, be small to avoid the formation of grain boundary carbide films, which are detrimental to creep resistance.<sup>13,19</sup> In this respect, 0.07 wt-% was considered an appropriate balance
- (v) boron, to segregate at grain boundaries by filling vacancies, which limits the grain boundary sliding mechanism.<sup>19,20</sup> Usual levels are around 0.005 wt-%
- (vi)  $\sim 5$  wt-% of iron, to reduce cost. Pure chromium is very expensive, so ferrochrome or industrial scrap, which are both cheaper sources of Cr, will be used instead
- (vii) a usual commercial alloy level of silicon, i.e. 0.4 wt-%, as a deoxidant.

Having fixed the contents of Cr, Fe, C, B, and Si, predictions were made with various amounts of W, Al, and Ti. The latter were adjusted to find a compromise



8 Predicted relationship between creep rupture stress of proposed alloy and its lifetime at 650 and 750°C

between high creep rupture resistance with low  $\gamma'$  volume fraction, a low  $\gamma/\gamma'$  lattice misfit, and no undesirable phase formation at the service temperature (750°C) (shown in Part 2 of this series<sup>23</sup>). The proposed composition (wt-%) was

Ni-20Cr-3.5W-2.3Al-2.1Ti-5Fe-0.4Si-0.07C-0.005B

Heat treatment consisted of (*see also* Part 2): 4 h at 1175°C, 4 h at 935°C and 24 h at 760°C, with air cooling in all cases.

## MECHANICAL PROPERTIES

The main mechanical properties of the proposed alloy, estimated using the Gaussian processes models, are presented in Figs 7 and 8.

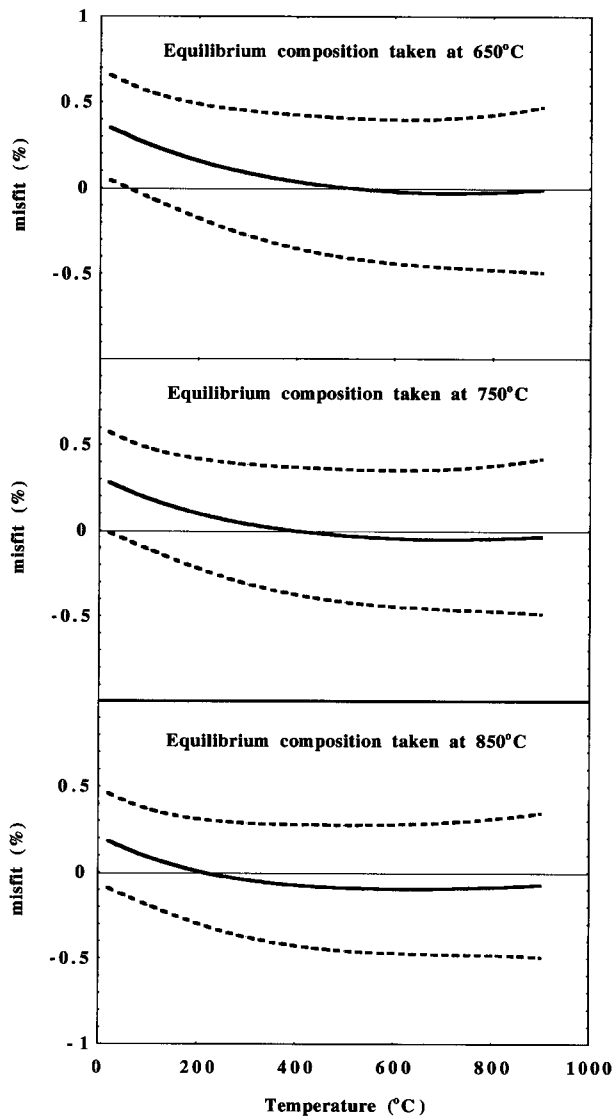
This alloy should have a yield stress of about 800 MPa  $\pm$  80 and a UTS of 1050 MPa  $\pm$  100 at room temperature and up to about 600°C, with the already discussed maximum in the yield stress as a function of temperature, resulting from the competition between softening of the  $\gamma$  matrix and hardening of the  $\gamma'$  phase (Fig. 7). The predicted UTS/Y ratio at room temperature is about 1.3, which is consistent with the design criterion.

As could be expected from the modelling and testing results, predicted ductility is associated with low confidence, i.e. large error bars. Nevertheless, assuming that the mean prediction is fair, the evolution of ductility with temperature follows a classical trend for a precipitation hardened superalloy: it first increases with temperature due to softening of the matrix, but then decreases at higher temperatures ( $\sim 600^\circ\text{C}$ ) because of the huge difference in the flow properties of  $\gamma$  and  $\gamma'$ , which causes early failure. It then increases strongly as the precipitates progressively dissolve and finally disappear above the  $\gamma'$  solvus (*see* Part 2).

The predicted relations between creep rupture stress and lifetime at 650°C and 750°C are also presented in Fig. 8. The novel alloy should meet the main design target of 100 MPa for 100 000 h at 750°C, and be more creep resistant at 650°C than the best performing power plant ferritic steel presently available.<sup>21</sup> However, it is worth noting that the exact composition of the proposed alloy has been adjusted for the design target at 750°C, and that it has been intentionally chosen that the mean prediction, and not the predicted lower bound, would match the design requirement. This has been done for reasons concerning phase stability at service temperature, which will be detailed in Part 2.<sup>23</sup>

## $\gamma/\gamma'$ LATTICE MISFIT

The equilibrium compositions of the  $\gamma$  and  $\gamma'$  phases at various temperatures have been estimated using the Thermo-Calc phase diagram simulation software,<sup>22</sup> whose



9 Predicted evolution with temperature of  $\gamma/\gamma'$  lattice misfit of proposed alloy.  $\gamma$  and  $\gamma'$  lattice parameters predicted with equilibrium compositions calculated at 650°C, 750 and 850°C

use is described in Part 2 of this series. These compositions have then been used as inputs in the  $\gamma$  and  $\gamma'$  lattice parameter Gaussian processes models, in order to estimate the  $\gamma/\gamma'$  lattice misfit in the material. The results are presented in Fig. 9. Although the calculated error bars are large, which results partly from the separate calculation of  $a_\gamma$  and  $a_{\gamma'}$ , the predicted lattice mismatch is small at the service temperature, even if the equilibrium compositions have been taken at 650 or 850°C. Small lattice mismatch is beneficial to creep resistance,<sup>11</sup> since it stabilises the  $\gamma/\gamma'$  interface and prevents  $\gamma'$  growth at elevated temperatures, and  $\gamma'$  rafting during creep.

## COST

Although the production cost of an alloy strongly depends on process, the first step in price reduction (which is the main goal of the present work) is to reduce the cost of its elements. This is why expensive elements have not been included in the proposed alloy design (Co, Mo, Ta, Nb...). In this respect, its elemental price, calculated from a list of relative element prices provided by Special Metals, is about 50% less than that of commercial alloys such as Inconel 617, Nimonic 115, or Nimonic PK33, and even 3% lower than

the price of Nimonic 80A, an alloy with significantly poorer mechanical properties.

## Conclusions

Gaussian processes have been used as quantitative tools to design a new and relatively cheap nickel base superalloy for power plant applications.

Using large databases containing information about many existing alloys and a Gaussian processes method, general models have been created describing the main mechanical properties and the  $\gamma/\gamma'$  lattice misfit of any alloy as functions of its composition, mechanical and/or heat treatment, and test conditions. After thoroughly testing these models, it was possible to use them to estimate the behaviour of new alloys. Following a careful review of the role and price of each alloying element, and of the industrial requirements in terms of mechanical properties, forgeability and weldability, a novel alloy has been proposed. The whole set of properties has been achieved using well balanced compositions excluding expensive elements such as Mo, Co, Ta, and Nb, so that the elemental cost of the designed alloy should be less than some of the cheapest commercial superalloys having significantly poorer mechanical properties.

However, because undesirable phases may form in this new alloy, a phase diagram and chemical segregation simulation method has been used in parallel with the Gaussian processes modelling of mechanical properties, and is presented in Part 2 of this series.

## Acknowledgements

The authors are grateful to the Engineering and Physical Sciences Research Council for funding this work, and to Alstom Power, Corus, Mitsui Babcock Energy Ltd., Rolls-Royce plc, Special Metals, and the University of Wales, Swansea, for partnership. The authors also thank Professor Colin Humphreys for all his support in the Technology Foresight Programme.

## References

1. C. A. L. BAILER-JONES, H. K. D. H. BHADSHIA and D. J. C. MACKAY: *Mater. Sci. Technol.*, 1999, **15**, 287–294.
2. F. TANCRET, H. K. D. H. BHADSHIA and D. J. C. MACKAY: *ISIJ Int.*, 1999, **39**, 1020–1026.
3. F. TANCRET, H. K. D. H. BHADSHIA and D. J. C. MACKAY: *Key Eng. Mater.*, 2000, **171–174**, 529–536.
4. C. A. L. BAILER-JONES, D. J. C. MACKAY, T. J. SABIN and P. J. WITHERS: *Austr. J. Intell. Inf. Process. Syst.*, 1998, **5**, 10–17.
5. M. N. GIBBS: 'Bayesian Gaussian processes for regression and classification', PhD thesis, University of Cambridge, UK, 1998.
6. C. K. I. WILLIAMS and C. E. RASMUSSEN: in 'Advances in neural information processing systems 8', (ed. D. S. Touretzky *et al.*); 1996, Cambridge, MA, MIT Press.
7. P. BEARDMORE, R. G. DAVIES and T. L. JOHNSTON: *Trans. AIME*, 1969, **245**, 1537–1545.
8. K. M. DELARGY, S. W. K. SHAW and G. D. W. SMITH: *Mater. Sci. Technol.*, 1986, **2**, 1031–1037.
9. D. RAYNOR and J. M. SILCOCK: *Met. Sci. J.*, 1970, **4**, 121–129.
10. A. P. MIODOWNNIK and N. SAUNDERS: 'Calculation of the APB energies in Ni-based superalloys', Report to Rolls-Royce plc (P24133).Thermotech Ltd, UK, 1993.
11. G. N. MANIAR and J. E. BRIDGE JR: *Metall. Trans.*, 1971, **2**, 95–102.

12. G. E. MAURER, L. A. JACKMAN and J. A. DOMINGUE: Proc. Conf. 'Superalloys 1980', Seven Springs, PA, USA, 1980, 43–52; 1980, Metals Park, OH, American Society for Metals.
13. T. MATSUO, M. UEKI, M. TAKEYAMA and R. TANAKA: *J. Mater. Sci.*, 1987, **22**, 1901–1907.
14. J. JONES: 'Neural network modelling of the tensile properties of nickel base superalloys', PhD thesis, University of Cambridge, UK, 1997.
15. Y. MISHIMA, S. OCHIAI, N. HAMAQ, M. YODOGAWA and T. SUZUKI: *Trans. Jpn Inst. Met.*, 1986, **27**, 656–664.
16. J. P. COLLIER, P. W. KEEFE and J. K. TIEN: *Metall. Trans. A*, 1986, **17A**, 651–661.
17. K. M. CHANG and A. H. NAHM: in 'Superalloys 718 – metallurgy and applications', (ed. E. A. Loria), 631–646; 1989, Warrendale, PA, TMS.
18. R. F. MILLER and G. S. ANSELL: *Metall. Trans. A*, 1977, **8A**, 1979–1991.
19. A. K. JENA and M. C. CHATURVEDE: *J. Mater. Sci.*, 1984, **19**, 3121–3139.
20. R. F. DECKER and J. W. FREEMAN: *Trans. AIME*, 1960, **218**, 277–285.
21. F. MASUYAMA: in 'Advanced heat resistant steel for power generation', (ed. R. Viswanathan and J. Nutting), 33–48; 1999, Cambridge, Cambridge University Press.
22. Thermo-Calc, The Royal Institute of Technology, Stockholm, Sweden.
23. F. TANCRET and H. K. D. H. BHADESHIA: *Mater. Sci. Technol.*, 2003, **19**, 291–295.